Published in final edited form as:
Biochemistry. 2011 June 21; 50(24): 5453–5464. doi:10.1021/bi101846x.

The E2 domains of APP and APLP1 share a conserved mode of dimerization

Sangwon Lee[1], **Yi Xue**[1], **Jian Hu**[1], **Yongcheng Wang**[1,#], **Xuying Liu**[1], **Borries Demeler**[2], and **Ya Ha**[1,*]

[1] Department of Pharmacology, Yale School of Medicine, New Haven, Connecticut 06520, USA

[2] Department of Biochemistry, the University of Texas Health Science Center at San Antonio, Texas 78229, USA

Abstract

Amyloid precursor protein (APP) is genetically linked to Alzheimer's disease. APP is a type I membrane protein, and its oligomeric structure is potentially important because this property may play a role in its function, or affect the processing of the precursor by the secretases to generate amyloid β-peptide. Several independent studies have shown that APP can form dimers in the cell, but how it dimerizes remains controversial. At least three regions of the precursor, including a centrally located and conserved domain called E2, have been proposed to contribute to dimerization. Here we report two new crystal structures of E2, one from APP, and the other from APLP1, a mammalian APP homolog. Comparison with an earlier APP structure, which was solved in a different space group, shows that the E2 domains share a conserved and anti-parallel mode of dimerization. Biophysical measurements in solution show that heparin binding induces E2 dimerization. The 2.1Å resolution electron density map also reveals phosphate ions that are bound to the protein surface. Mutational analysis shows that protein residues interacting with the phosphate ions are also involved in heparin binding. The locations of two of these residues, Arg-369 and His-433, at the dimeric interface suggest a mechanism for heparin-induced protein dimerization.

Amyloid precursor protein (APP) has generated great interest in both medical and basic research. Mutations in APP are known to cause familial Alzheimer's disease (for a recent review, see ref. 1), yet the physiological function of the precursor protein remains elusive. In mammals APP has two homologs, APLP1 and APLP2 (2, 3). Knocking out all three genes is lethal to the animal (4). APP and the two APLPs are type-I membrane proteins (5), and are found both inside the cell and on the cell surface. Proteolysis by secretases releases various fragments of the protein from the membrane. These include amyloid β-peptide, widely believed to play an important role in Alzheimer's disease (6), a number of different ectodomain fragmenets that have been shown to have various biological activities (e.g., see ref. 7–9), and a small intracellular domain that is thought to function in transcriptive regulation (e.g., see ref. 10–12).

[*]Corresponding author: Ya Ha, Ph.D., Department of Pharmacology, Yale School of Medicine, 333 Cedar Street, New Haven, Connecticut 06520, USA. Tel.: 203-785-7530, Fax: 203-785-7670, ya.ha@yale.edu.
[#]Present address: Monsanto Company, 700 Chesterfield Parkway West, Chesterfield, Missouri 63017, USA

The atomic coordinates and structure factors (code 3NYJ and 3PMR) have been deposited in the protein data bank, Research Collaboratory for Structural Bioinformatics, Rutgers University, New Brunswick, NJ (http://www.rcsb.org/).

Supporting Information Available: supplemental figures S1–S7: the anomalous Fourier maps for APP showing Se peaks and Os binding sites, the electron density maps for the loop between αD and αE, a sequence alignment, an electron density map showing the domain-swapped feature of APLP1, the difference Fourier map showing the bound phosphate ions, and the fluorescence and AUC data of APLP1 in the presence of other polyanions. This material is available free of charge via the Internet at http://pubs.acs.org.

The oligomeric structure of APP is potentially important because this may affect its proteolytic processing (13), or play a role in the transmembrane signaling mechanism that the protein is involved in (14). Biochemical and cell biological studies have shown that APP can form dimers in the cell (14–18), but many questions remain controversial. For example, which domain of the membrane protein is responsible for dimerization (16, 19, 20)? Is dimerization obligatory, or induced by ligand binding (e.g., heparan sulfate proteoglycans; ref. 20, 21)? The matter is further complicated by the possibilities that APP may heterodimerize with the APLPs, and that dimerization can occur not only *in cis*, but also *in trans* between molecules from different cells (16, 18).

The ectodomains of APP and APLPs have two conserved regions called E1 and E2 (Fig. 1A), both of which have been proposed to contribute to dimerization. A recently solved crystal structure of E1 reveals an interesting dimeric arrangement of the protein where the dimeric contact is mediated exclusively through the N-terminal portion of the molecule, a substructure called the growth-factor-like-domain (GFLD) (20). In an earlier study, however, the isolated GFLD crystallized as monomers (22). The crystal structures of E2 (19, 23), and the NMR structure of a fragment of it (24), have also been solved. The crystal structure shows that E2 forms an antiparallel dimer (19). Nevertheless, the hypothesis that E2 may function as the dimerization domain of the full-length molecule was recently challenged by the observation that the E2 domain of the *C. elegans* homolog APL-1 has been crystallized as monomers (25). To help clarify the oligomeric structure of E2, here we report two new crystal structures of E2, one from APP and the other from APLP1, and show that they share the same mode of antiparallel dimerization. We also show for the first time that heparin binding induces E2 dimerization. Since the APP family of proteins travels to cell surface, and can be secreted into the extracellular matrix, the possibility that heparan sulfate proteoglycans might modulate their oligomerization states has important biological implications.

Materials and Methods

Subcloning, protein expression and purification

The procedures for the expression and purification of native and Se-Met substituted APP (construct $APP_{346–548}$) have been described previously (19). Full-length cDNA for human APLP1 was purchased from Open Biosystems (MHS1010-74392). A total of six E2 constructs of APLP1 were made based on sequence alignment with APP (19). They differed from each other by a few amino acids at either the N- or C-terminus. The constructs were subcloned into vector pET28a (Novagen) at the NdeI and XhoI restriction sites. Recombinant protein was expressed in BL21-Gold(DE3) cells (Agilent Technologies) grown in LB media. After induction with 0.5 mM IPTG at OD_{600} 0.5, cell culture was continued for 18 hrs at room temperature. Harvested cells were re-suspended in a buffer containing 20 mM sodium phosphate (pH 7.8), 500 mM sodium chloride, and cOmplete protease inhibitor cocktail (Roche), and lysed by freeze and thaw in the presence of lysozyme. The recombinant protein was purified from the lysate using Talon affinity chromatography (Clontech). The N-terminal hexa-Histidine tag was removed by thrombin after overnight dialysis of the recombinant protein against the gel filtration buffer (20 mM HEPES pH 7.5, 500 mM NaCl, 5% glycerol). Thrombin-treated protein was concentrated and passed through a Superdex S-200 column (GE healthcare). The mono-dispersed peak was collected for later studies. Mutants were generated by the QuikChange method of site-directed mutagenesis according to the protocol supplied by the manufacturer (Agilent Technologies). They were expressed and purified similarly.

Crystallization and structure determination of APP

Plate-like crystal clusters could be readily generated by hanging drop method by mixing 1μl 10mg/ml protein solution in a buffer of 10mM HEPES pH 7.5 with 1μl well solution of 12% PEG 4,000, 20% isopropanol and 0.1M Na citrate pH 5.6. Single crystals were cut from the cluster, and cryoprotected in 30% PEG 400. The native crystal diffracted to 3.2Å resolution, but the diffraction was anisotropic and tended to produce streaky spots. After screening many crystals, a complete native dataset was collected from a single and best-diffracting crystal to 3.4Å resolution. The molecular replacement program *phaser* (26) found a clear solution by using two search models, each presenting the N- and C-terminal subdomains of the known E2 structure (PDB 1rw6), respectively. Refinement was, however, difficult as the electron density map showed very few new features based on which the model could be improved (the initial R factor was around 0.47). Density modification was not useful because the solvent content of the crystal was normal (~51%) and there was no non-crystallographic symmetry averaging. After rounds of refinement, the R/R_{free} values remained high (0.41/0.44). We decided then to try and obtain experimental phases. The Se-Met substituted protein turned out to produce slightly better diffracting crystals, and cryoprotection by paratone oil was found to be better and more reproducible. Two highly redundant Se-MAD datasets were collected. Unfortunately, they failed to generate useful phase information even with the known Se sites, which could be obtained from the molecular replacement solution. We noticed that our crystallization condition was similar to that reported by Keil et al. (2004), who were successful in derivatizing APP crystals with $(NH_4)_2OsCl_6$ (their protein construct was longer, and crystallized in a different space group) (23). We soaked our Se-Met crystals in 5mM $(NH_4)_2OsCl_6$ overnight before transferring them to paratone oil and flash freezing in liquid nitrogen. A 3.2Å resolution dataset was collected at the Os peak wavelength (1.1400Å) at beamline X29 of BNL-NSLS. Program *hkl2map* (27) was able to find the single Os site, but the electron density map based on SAD phasing was again not interpretable. Due to the lack of isomorphism, the attempt to obtain phases by SIRAS, using the Os data and a “native” Se-Met dataset collected at the same wavelength, also failed. Since the 3.2Å resolution Os dataset was better in quality than the earlier native dataset, and produced clearer maps, we used it to conduct molecular replacement and refinement again. This time we used an ensemble of three structures (APP, APL-1 and APLP1) that have now become available to emphasize features common to this family of proteins. The first short helix αA was removed from the N-terminal search probe due to clashes with a neighboring molecule. *Phaser* found the same molecular replacement solution, but the resulting electron density map was more meaningful, revealing many differences between the real structure and the search probe. To ensure that the molecular replacement solution was correct, difference anomalous Fourier map was calculated from a dataset collected from a Se-Met crystal at the Se peak wavelength (0.9792Å), which revealed strong peaks that matched perfectly with six of the nine methionines in E2 predicted by the molecular replacement solution (supplemental Fig. S1). The peaks were of different heights (the two N-terminal methiones were 8σ above background), reflecting different degrees of motion. At 4σ, no other peaks were visible in the map. Anomalous difference Fourier map calculated from the Os dataset revealed a single 14σ peak situated between the two subdomains of E2 that corresponded to the bound metal ion (supplemental Fig. S2A). The coordinates of the bound Os (-0.5726, 0.1249, 0.2758) were consistent with peaks observed in anomalous Patterson map, which was independently calculated (supplemental Fig. S2B). Supplemental Fig. S3 compared a region of the electron density map showing how helices αD and αE were differently connected in the new structure: a poorly defined and extended segment from His-495 to Met-498 had now become a continuation of the αD helix; to bridge the gap between the two helices, a short segment of helix αE, from Pro-501 to Gln-506, had bent sharply towards αD, creating a kink after Gln-506. The new structure was now more similar to that of APLP1 at this region (both had

the kink after Gln-506). The model had an R factor initially around 0.46. After cycles of refinement by *CNS* and *refmac5* (28, 29), and manual adjustments using program *O* (30) based on 2fo-fc and fo-fc maps, we refined the structure to an R/R_{free} of 0.29/0.37 with reasonable geometry (Table 1). Further improvement was hindered by resolution, and by disorders that appeared to be intrinsic to this crystal form, which rendered some parts of the structure difficult to visualize. The overall temperature factor was high (102 $Å^2$). Electron density was particularly poor near the two termini (αA, αF), and at the loop between αC and αD. About 20% of the side chains remained missing in the final electron density map.

A comparison with the high resolution APLP1 structure (see below) suggested that a few changes need to be made to the original APP structure, which was also solved at a medium-to-low resolution (19). The changes involved the ends of the molecule that were poorly defined in the electron density map. Near the N-terminus, the loop between helices αA and αB was rebuilt so that Tyr-359 now pointed inward to hydrogen bond with Glu-368 and Arg-441. Towards the C-terminus, a remodeled loop before helix αF would enable Ile-539 to make hydrophobic contacts with Val-471, Phe-472 and Leu-529. After incorporating the changes, the R/R_{free} of the model improved from 0.274/0.342 to 0.258/0.322. The improved coordinates have also been deposited in PDB (accession number 3NYL).

Crystallization and structural determination of APLP1

Crystallization conditions were initially screened in 96-well sitting drop plates using commercial kits Crystal Screen, Index, SaltRx, PEG/Ion (Hampton Research), and Wizard (Emerald Biosystems). All six constructs produced crystals most of which showed the morphology of needle clusters. After optimization, single rod-like crystals were obtained from construct $APLP1_{285–499}$ when a 7 mg/ml protein solution in 20 mM HEPES pH 7.5, 5% glycerol was mixed with an equal volume of well solution containing 1.26 M Na_2HPO_4, 0.14 M KH_2PO_4 at pH 5.6 and equilibrated for 4–7 days using sitting drop vapor diffusion method. The crystals were cryo-protected in 100% Paratone-N (Hampton Research) before being flash-frozen in liquid nitrogen. X-ray diffraction data were acquired at the Brookhaven National Synchrotron Light Source beamline X29, and processed with *HKL2000* (31). The structure was again solved by *phaser*: since there were two copies of E2 in the asymmetric unit, and the two subdomains in each polypeptide chain were flexible, the program had to locate four search models (both subdomain models were an ensemble of human APP and worm APL-1 structures) (19, 25). The model phase was significantly improved by the independent 2-fold averaging of the N- and C-terminal subdomains (the symmetry operators for the two subdomains were different by 5 degrees). Based on the density-modified map, an almost complete model for APLP1 could be confidently built (including retracing of the domain-swapped loop and helix αA) using *coot* (32). After two rounds of model building and refinement by *CNS* (28), the R/R_{free} dropped to 0.286/0.308. At this stage, the difference map was inspected, which clearly revealed four bound phosphate ions (supplemental Fig. S7). Adding the phosphate ions to the protein model, and auto-picking water molecules, further reduced the R-value, and improved the clarity of the map. The final step of refinement was carried out using *refmac5* (29) (Table 1).

Analytical ultracentrifugation

All experiments were performed on a Beckman Optima XL-I at the Center for Analytical Ultracentrifugation of Macromolecular Assemblies (CAUMA) at the University of Texas Health Science Center at San Antonio. Sedimentation velocity (SV) data were analyzed with *UltraScan* (33, 34). Calculations were performed at the Texas Advanced Computing Center at the University of Texas at Austin, and at the Bioinformatics Core Facility at the University of Texas Health Science Center at San Antonio as described in (35). Both APP and APLP1 were prepared in a buffer containing 10mM sodium phosphate, 10mM sodium

acetate and 50mM NaCl (pH 7.5). The protein:heparin complexes were prepared in the same buffer plus 100μM heparin (average M.W. 5,000 Da; Santa Cruz Biotechnology). The data were measured in intensity mode at 230nm and 280nm, at 20ºC, and at 45 krpm, using standard epon 2-channel centerpieces. The protein concentrations for samples measured at 230nm were about 3.2μM (OD_{230nm}=0.31), those measured at 280nm ranged from 28μM (OD_{280nm}=0.32) to 66μM (OD_{280nm}=0.76). Partial specific volumes of APP and APLP1 were determined to be 0.729 and 0.728 cm^3/g, respectively. Data were first analyzed by two-dimensional spectrum analysis with simultaneous removal of time-invariant noise (36, 37), and then by enhanced van Holde–Weischet analysis (38) and genetic algorithm refinement (39, 40), followed by Monte Carlo analysis (41).

Fluorescence spectroscopy

The fluorescence measurements were performed using a spectrofluorometer from Photon Technology International. The excitation wavelength was set at 295nm and the emission spectra were recorded from 300nm to 450nm with 1nm interval at the speed of 1nm/sec. A total of three scans were acquired and averaged. The protein solutions were in 20mM phosphate buffer (pH 7.5) and the protein concentration was 3μM. The protein: heparin complexes were prepared in the same buffer plus 6μM heparin (average M.W. 5,000 Da; Santa Cruz Biotechnology). The emission spectra of free tryptophan, which were recorded similarly, were not affected by the presence of heparin.

Heparin affinity chromatography

All protein samples were dialyzed against a buffer containing 10mM sodium phosphate and 10mM sodium acetate (pH 7.5). The protein sample was applied to a 1mL Hi-Trap Heparin HP column (GE healthcare) equilibrated with the same buffer, and eluted by a linear concentration gradient (0.0 M to 2.0 M) of NaCl.

Results

The structure of APP E2 domain in a new crystal form

To address the question of whether the E2 dimer observed in the previous APP structure could result from crystallization, we have now found a new crystal form of APP (crystal form “B”), which is based on a slightly shorter E2 construct, and was obtained from a different crystallization condition (polyethylene glycol instead of salt). The new structure was solved by molecular replacement (table 1). Although poor diffraction and disorder had rendered refinement difficult, the molecular replacement solution has to be correct: it can be used to accurately locate six of the nine selenium atoms, and an osmium atom, from Se-Met and Os-derivatized crystals by anomalous Fourier analysis using diffraction data collected at Se or Os absorption edges (supplemental Figs. S1 and S2); it also produces clear electron densities for parts of the protein structure that are either disordered or different in the search probe (supplemental Fig. S3). One polypeptide chain is present in the asymmetric unit of the crystal. It is closely packed against a second molecule related by crystallographic 2-fold symmetry to form a dimer, in an anti-parallel manner similar to that observed in the first crystal form (Fig. 1B). The anti-parallel dimers, now observed twice, and their overall similarities can not be coincidental, especially when their crystal packing environments are completely different. In the following sections we will describe a third E2 dimer structure (that of APLP1), which is determined at a much better resolution and properly refined, and show that it not only shares the same mode of dimerization, but also demonstrates similar conformational flexibilities.

The structure of APLP1 E2 domain

The E2 domain of APLP1 shares 51% sequence identity with the E2 domain of APP (supplemental Fig. S4). Assisted by multi-domain averaging, its structure can also be solved by molecular replacement (Table 1): the electron density map calculated after density modification was of very high quality, revealing most of the differences between APLP1 and the search probe; it also became clear that the first α-helix (αA) of both copies of E2 in the asymmetric unit had domain-swapped with a neighboring molecule (supplemental Fig. S5A-B). In the two previously known E2 structures (19, 25), αA is packed to the side of αB and αC, which brings together four completely conserved residues (Tyr-297, Glu-306, His-376 and Arg-379) to form a network of hydrogen bonds (supplemental Fig. S5C-D). All these interactions are maintained in the domain-swapped APLP1 structure (with the exception that Tyr-297 now comes from a separate polypeptide chain). The swapping is made possible by two glycyl and one prolyl residues in the short loop that connects αA to αB. Most illustrations of APLP1 in this paper have αA modeled back to its original position.

There are two copies of E2 in the asymmetric unit of APLP1 crystal that are related roughly by a 2-fold rotation (Fig. 1C). The two E2s form a tightly associated dimer that is quite similar to the E2 dimer of APP described above. The corresponding helices in the two E2s are pointing in opposite directions, and the N-terminal subdomain of one monomer is packed against the C-terminal subdomain of the second monomer, burying an identical set of conserved hydrophobic residues (see below). The αB and αC helices in APLP1, however, are more tilted outwards. This is accompanied by rotations of αD and αE in its dimerization partner to maintain contact. As a result of these movements, the dimeric structure of APLP1 appears less compact, and contains a large hole in the middle that connects the front of the molecule to the back.

Conformational flexibilities within the monomer

When the two APP structures are superimposed on C-terminal subdomain, the N-terminal subdomain of the new structure appears to have bent significantly outward by about 15 degrees (Fig. 2A). The flexibility is achieved by small dihedral angle changes in a short stretch of residues around Arg-441 near the middle of the long αC helix. Since there is little contact between the two subdomains within the monomer (the only interaction lost in the new structure is a hydrogen bond between Glu-436 and His-492), their relative orientation has to be maintained by the continuity of the long helix αC that spans the length of the molecule. The fact that Arg-441 is partially cleavable by trypsin in solution (when the molecule is monomeric; see below) suggests that the long helix can sometimes unwind in the middle, which would probably enable the N-terminal subdomain to bend further than illustrated by the current structures (24).

The structures of the two subdomains in APLP1 are very similar to those in APP: their helices (63 Cα atoms from the N-terminal subdomain and 74 Cα atoms from the C-terminal subdomain) are superimposable with r.m.s. deviations of 0.70Å and 1.08Å, respectively. The largest difference between APLP1 and APP is again in the inter-subdomain angle: the N-terminal subdomain of APLP1 is tilted further away from the C-terminal subdomain by about 31 degrees (black and red in Fig. 2B). The two copies of E2 in the asymmetric unit of the APLP1 crystal are not exactly identical: they differ also in the inter-subdomain angle by about 5 degrees (black and blue in Fig. 2B).

Conformational flexibilities within the dimer

Despite the large movement between the two subdomains (Fig. 2A), the dimerization interface is maintained. Fig. 3A compares the two APP structures at one of the two identical interfaces (the region boxed in Fig. 3C), where the N-terminal helical hairpin (αB, αC)

crosses over a pair of C-terminal helices (αD, αE): by superimposing the structures on the C-terminal helices, αB/αC of the new structure appear to have rotated downward, creating a wider gap with αD/αE. Most interactions at the interface are changed by this movement with the exception of the hydrophobic contacts between a pair of highly conserved leucines (Leu-490*, Leu-515*) on αD/αE and a string of three hydrophobic residues (Met-387, Met-391, Trp-394) on αB. The lack of any strong interactions may account for the flexibility observed at the interface.

The bending of the N-terminal subdomain at the tertiary structural level and the rotation at the dimeric interface are mechanically coupled (Fig. 2A; Fig. 3A). The movements of individual subdomains within the dimer can be simulated by the model depicted in Fig. 3D. In this model, the subdomains from the two monomers are joined at “b” (open circle), and can only rotate about it. Any rotation around “a” (grey circle) inevitably leads to a rotation around “b”, in the direction that is consistent with the crystallographic observation. In the real structure, the contact between Met-387 and Leu-490*, which remains unchanged in the two structures (αB and αC appear to pivot around Met-387), would be equivalent to point “b” in the model.

The “movement” of helices in APLP1, when compared to APP, is strikingly similar to that between the two APP crystal forms (except that the difference is bigger; Fig. 3B). As also shown in Fig. 3C, the N-terminal and C-terminal subdomains of APLP1 are similarly packed but have a wider angle between them. The dimeric interface involves an identical pair of conserved leucines on αD and αE (Leu-428*, Leu-453* in APLP1 numbering). Although αB has now moved to the lower side the leucines, Ile-325 and Met-329 (equivalent to Met-387 and Met-391 of APP) remain in hydrophobic contacts with them. These comparisons suggest that individual subdomains in the APLP1 dimer structure are similarly coupled so that, during the course of evolution, their movements are restrained by the same type of requirements to maintain dimeric contact.

Heparin binding alters E2 monomer: dimer equilibrium

The oligomeric structure of the E2 domains in solution was studied by analytical ultracentrifugation (AUC), using sedimentation velocity (SV) experiments as described in (42). A concentration series of APLP1 was analyzed with the enhanced van Holde-Weischet method (38), and revealed a mass-action effect suggesting the presence of a monomer to dimer equilibrium (Fig. 4A): while essentially monomeric at 3μM, at 66μM the s-value distribution was shifted considerably to the dimeric state. Whole boundary modeling of two separate high concentration experiments with a reversible model for the Lamm equation (43) as described in (42) resulted in two equivalent fits, which indicated a weak, but rapidly reversible monomer to dimer equilibrium (K_d=161μM [144.2, 182.7], k_{off} ≥0.003/sec). Heparin altered this equilibrium significantly. Even at 3μM E2 concentration, the presence of 100μM heparin shifted the van Holde-Weischet integral s-value distributions, suggesting higher oligomerization states (Fig. 4B). Plots of genetic algorithm-Monte Carlo analyses using non-interacting models for these data clearly show an increase in the partial concentration of a higher molecular weight species, which is consistent with E2 dimer formation (Fig. 4C-F). To further quantify the degree of this association, we fitted the heparin data to reversible monomer-dimer association models as described in (42). These fits resulted in K_d values of 9.2μM [8.1, 10.7] for APP, and 7.8μM [6.8, 9.3] for APLP1, suggesting a significantly tighter dimerization than that observed for APLP1 without heparin. Taken together, these analyses demonstrated for the first time that heparin binding to E2 shifts the association/dissociation equilibrium in favor of dimer formation, and confirmed our earlier hypothesis that E2 dimerization is a dynamic and reversible process (19, 25).

The E2 domain of APLP1 contains a single tryptophan residue (Trp-332). Adding heparin to the protein solution causes a 60% drop of the protein's fluorescent intensity (Fig. 4G). This effect is specific to heparin since other polyanions such as sucrose octasulfate (a heavily sulfated disaccharide) and chondroitin sulfate (which is similar to heparan sulfate but has galactosamine residues instead of glucosamines in its backbone) do not change the protein's fluorescent properties (Fig. S7). Since Trp-332 is far from the known heparin binding site on E2, thus unlikely to be directly affected by the ligand, the change of its fluorescent property must result from protein dimerization (or a conformational change that is associated with dimerization). This is consistent with the observation that Trp-332 is found at the dimeric interface of the crystal structures (blue open circles in Fig. 3B). The binding of heparin to APP also causes a change in protein fluorescence, but the amplitude of the change is smaller (data not shown).

Heparin may induce protein dimerization through at least one of two possible mechanisms. In one mechanism, the protein protomers are bridged by the ligand, but do not interact with each other directly (Fig. 4H). This is possible especially because heparin is a linear polymer with many repeating disaccharide units and both sides of the sugar can bind proteins. At higher ligand concentrations, however, the dimer is expected to break apart readily so that each protein protomer can bind a separate ligand molecule. In the second mechanism, dimerization involves extensive protein:protein contact (Fig. 4I). Heparin binding may modify the surface property of the monomeric protein, rendering it complementary for dimer formation. The AUC experiments depicted in Figs. 4D and 4F were conducted in the presence of excessive amount of heparin (~30 times the protein concentration). The fact that the complex was mostly dimeric under this condition seems to suggest that the heparin-induced E2 dimer is stabilized by not only protein:heparin but also protein:protein interactions (Fig. 4I).

The influence of heparin on E2 dimerization can be envisioned in a different but thermodynamically equivalent way (Fig. 4I). E2 may dimerize in the absence of heparin, although equilibrium favors dissociation. If the ligand has a higher affinity for the dimeric E2, its presence will deplete the empty dimers, and re-establish the equilibrium by drawing more monomers into dimers. The crystallization process, which takes place at high protein concentrations, may similarly favor the formation of dimers.

Phosphate binding sites

The two previously solved E2 structures were of only medium resolution (19, 25). The high resolution of the APLP1 structure permits not only visualization of most protein side chains, but also accurate modeling of bound solvent molecules. In the difference Fourier map, there are four prominent peaks (7–11σ; supplemental Fig. S6). These peaks are related roughly by the non-crystallographic 2-fold symmetry, and appear next to positively charged protein side chains. They must correspond to heavier phosphate ions, which are abundantly present in the crystallization solution (the protein is crystallized in 1.4M Na/K phosphate). One phosphate (P1) interacts with Lys-422, Arg-425 and Arg-429 from helix αD, and the second phosphate (P2) is hydrogen bonded to His-433 and Gln-432 from the same helix, and to Lys-314* (via a water) and Arg-369* from the dimerization partner (Fig. 5A). The proximity of the bound phosphates to previously mapped heparin binding site led us to test whether the phosphate binding sites are also involved in heparin binding (Lys-422 is already known to bind heparin; see ref. 19, 25) (Fig. 5B). Arg-429, His-433 and Arg-369 were chosen for mutagenesis because they are highly conserved, and interact directly with the phosphates. As shown in Fig. 6B, R429A, H433A and R369A all elute earlier from a heparin column than the wild-type protein, confirming that these residues indeed participate in heparin binding.

The finding that heparin may interact with residues at the P2 binding site was not expected. Our previous work has established that His-307, His-426, Arg-418 and Lys-422 are involved in heparin binding (colored in blue in Fig. 6A) (25). The shallow pocket defined by these residues is readily accessible from the front of the molecule (Fig. 5B). The P2 binding site, however, is located much deeper towards the back of the molecule (yellow and green in Fig. 6A). To reach the P2 binding site from the front, the bulky heparin chain has to go through the narrow space between the two subdomains. It is therefore tempting to speculate that the binding of heparin to the deep groove between the two subdomains may restrict their rotational freedom and thereby promote dimerization. The simultaneous binding of heparin to residues from both polypeptide chains (e.g., His-433 and Arg-369*) may also directly strengthen the dimeric interface. To test this hypothesis, we examined the dimerization effect of heparin on the three mutant proteins generated above. As shown in Fig. 7A-C, when heparin was added to the protein solutions, the decrease of fluorescence intensity for the mutant proteins was less than that for the wild-type protein, suggesting a lesser degree of dimerization. Among the three mutants, R429A had the lowest affinity for heparin (Fig. 6B), and under our experimental conditions, heparin almost completely failed to induce its dimerization (Fig. 7B).

Discussion

We draw three general conclusions about the oligomeric structure of E2 from the present study. First, E2 can reversibly dimerize in solution. In the absence of ligand, however, the monomer predominates thermodynamically. This is probably true for all APP family members (25; our unpublished data). The techniques we used previously to analyze the oligomeric structure of E2 (size exclusion chromatography, dynamic light scattering) were inaccurate because the molecule has a very elongated shape (19). The new conclusion is consistent with the observation made by Gralle et al. showing that the secreted APP ectodomain as a whole, which contains not only E2 but also other domains, is also monomeric in solution (21). Secondly, we show for the first time that heparin binding causes E2 to dimerize. The dimerization of APP at the E2 domain can have many types of functional consequences. For example, dimerization may mask epitopes that potentially have biological activities. In the dimer structure, the RERMS sequence motif (APP_{751} residues 384–388), previously found to have growth promoting activities in cell culture (7, 44, 45), and a possible collagen binding site (residues 504–521) (46), are buried at the interface and not available for interaction with other proteins. The dimerization of the membrane-spanning APP (or its dissociation) may also serve as a mechanism to send signals into cells (14). Thirdly, the E2 domains appear to share a conserved mode of dimerization. This is based primarily on the crystallographic observation that, of the four E2 structures solved to date, three are dimeric and have similar structures. Only the E2 domain of the worm APL-1 was crystallized as monomers (25). Furthermore, we showed that residues located at the dimer interface are highly conserved (19).

We can not yet explain how heparin binding induces E2 dimerization. The most straightforward approach to address this question would be to try to co-crystallize the E2:heparin complex, but this effort has not been successful. Based on the hypothesis illustrated by Fig. 4I, one may predict that the crystallized E2 dimer should represent the form of the protein that has a higher affinity for the ligand. Therefore, direct soaking of heparin into the protein crystal offers another possible solution to the problem. The present crystallization condition for APLP1 (1.4M Na/K phosphate) prohibits heparin binding. We recently found a new condition for crystallizing APLP1 in polyethylene glycol, and preliminary x-ray diffraction analysis indicated that it also contains the dimeric protein. We are currently preparing this crystal form for soaking experiment: if the dimer observed in the crystal is different from that induced by heparin binding in solution (we can not yet rule out

this possibility definitively), heparin may fail to bind to the protein, or bind to a region of the protein that is inconsistent with the mutagenesis data.

Gralle et al. found that heparin induces dimerization of the full-length APP ectodomain (21). The results we present here could be interpreted as an indication that the dimerization may take place at the centrally located E2 domain. Recently, however, Dahms et al. reported that heparin can also induce dimerization of the E1 domain (20), which is located at the N-terminus of the full-length protein and separated from E2 by an acidic and probably unstructured segment of about 100aa (and, in some isoforms, an additional small protease inhibitor domain). Although small-angle x-ray scattering experiment has provided some general idea about the overall shape of the full-length molecule and its complex with heparin (21), one has to caution that the relative positions of E1 and E2 can not be accurately determined by this technique. Therefore, we can not exclude the possibility that E1 and E2 may both contribute to dimerization in a cooperative manner (this is not entirely impossible because E1 and E2 are separated by a long and flexible linker). Since E2 appears to have a higher affinity for heparin (47), it can even be speculated that it may represent the first site of protein:protein contact before E1 becomes involved.

Supplementary Material

Refer to Web version on PubMed Central for supplementary material.

Acknowledgments

Funding Information: This work was supported by NIH grant GM077547 (Y.H.). The ultracentrifugation analyses were supported in part by NIH grant RR022200 (B.D.). Supercomputer allocations were provided by National Science foundation TG-MCB070038 (B.D.).

We thank J. Schlessinger for allowing us to use the spectrofluorometer in his laboratory. We also thank H. Robinson and A. Saxena at NSLS-X29 for assistance during x-ray diffraction data collection. Financial support for the beamline comes principally from US Department of Energy, and from the National Institutes of Health. We thank Mr. Virgil Schirf for performing the AUC experiments at CAUMA, which is funded in part by the UTHSCSA Cancer Therapy and Research Center through the NIH-NCI P30 award CA054174, as well as by Texas State funds provided through the Office of the Vice President for Research of the UTHSCSA.

Abbreviations

APLP	APP-like protein
APP	amyloid precursor protein
AUC	analytical ultracentrifugation
GLPD	growth-factor-like-domain
SV	sedimentation velocity

References

1. Bettens K, Sleegers K, Van Broeckhoven C. Current status on Alzheimer disease molecular genetics: from past, to present, to future. Hum Mol Gen. 2010; 19:R4–R11. [PubMed: 20388643]
2. Wasco W, Bupp K, Magendantz M, Gusella JF, Tanzi RE, Solomon F. Identification of a mouse brain cDNA that encodes a protein related to the Alzheimer disease-associated amyloid beta protein precursor. Proc Natl Acad Sci U S A. 1992; 89:10758–10762. [PubMed: 1279693]
3. Wasco W, Gurubhagavatula S, Paradis MD, Romano DM, Sisodia SS, Hyman BT, Neve RL, Tanzi RE. Isolation and characterization of APLP2 encoding a homologue of the Alzheimer's associated amyloid beta protein precursor. Nat Genet. 1993; 5:95–100. [PubMed: 8220435]

4. Herms J, Anliker B, Heber S, Ring S, Fuhrmann M, Kretzschmar H, Sisodia S, Muller U. Cortical dysplasia resembling human type 2 lissencephaly in mice lacking all three APP family members. EMBO J. 2004; 23:4106–4115. [PubMed: 15385965]
5. Kang J, Lemaire HG, Unterbeck A, Salbaum JM, Masters CL, Grzeschik KH, Multhaup G, Beyreuther K, Muller-Hill B. The precursor of Alzheimer's disease amyloid A4 protein resembles a cell-surface receptor. Nature. 1987; 325:733–736. [PubMed: 2881207]
6. Hardy J, Selkoe DJ. The amyloid hypothesis of Alzheimer's disease: progress and problems on the road to therapeutics. Science. 2002; 297:353–356. [PubMed: 12130773]
7. Ninomiya H, Roch JM, Sundsmo MP, Otero DA, Saitoh T. Amino acid sequence RERMS represents the active domain of amyloid beta/A4 protein precursor that promotes fibroblast growth. J Cell Biol. 1993; 121:879–886. [PubMed: 8491779]
8. Quast T, Wehner S, Kirfel G, Jaeger K, De Luca M, Herzog V. sAPP as a regulator of dendrite motility and melanin release in epidermal melanocytes and melanoma cells. FASEB J. 2003; 17:1739–1741. [PubMed: 12958194]
9. Nikolaev A, McLaughlin T, O'Leary DD, Tessier-Lavigne M. APP binds DR6 to trigger axon pruning and neuron death via distinct caspases. Nature. 2009; 457:981–989. [PubMed: 19225519]
10. Cao X, Sudhof TC. A transcriptionally correction of transcriptively active complex of APP with Fe65 and histone acetyltransferase Tip60. Science. 2001; 293:115–120. [PubMed: 11441186]
11. Baek SH, Ohgi KA, Rose DW, Koo EH, Glass CK, Rosenfeld MG. Exchange of N-CoR corepressor and Tip60 coactivator complexes links gene expression by NF-kappaB and beta-amyloid precursor protein. Cell. 2002; 110:55–67. [PubMed: 12150997]
12. Pardossi-Piquard R, Petit A, Kawarai T, Sunyach C, Alves da Costa C, Vincent B, Ring S, D'Adamio L, Shen J, Muller U, St George Hyslop P, Checler F. Presenilin-dependent transcriptional control of the Abeta-degrading enzyme neprilysin by intracellular domains of betaAPP and APLP. Neuron. 2005; 46:541–545. [PubMed: 15944124]
13. Eggert S, Midthune B, Cottrell B, Koo EH. Induced dimerization of the amyloid precursor protein leads to decreased amyloid-beta protein production. J Biol Chem. 2009; 284:28943–28952. [PubMed: 19596858]
14. Gralle M, Botelho MG, Wouters FS. Neuroprotective secreted amyloid precursor protein acts by disrupting amyloid precursor protein dimers, The. J Biol Chem. 2009; 284:15016–15025. [PubMed: 19336403]
15. Scheuermann S, Hambsch B, Hesse L, Stumm J, Schmidt C, Beher D, Bayer TA, Beyreuther K, Multhaup G. Homodimerization of amyloid precursor protein and its implication in the amyloidogenic pathway of Alzheimer's disease. J Biol Chem. 2001; 276:33923–33929. [PubMed: 11438549]
16. Soba P, Eggert S, Wagner K, Zentgraf H, Siehl K, Kreger S, Lower A, Langer A, Merdes G, Paro R, Masters CL, Muller U, Kins S, Beyreuther K. Homo- and heterodimerization of APP family members promotes intercellular adhesion. EMBO J. 2005; 24:3624–3634. [PubMed: 16193067]
17. Munter LM, Voigt P, Harmeier A, Kaden D, Gottschalk KE, Weise C, Pipkorn R, Schaefer M, Langosch D, Multhaup G. GxxxG motifs within the amyloid precursor protein transmembrane sequence are critical for the etiology of Abeta42. EMBO J. 2007; 26:1702–1712. [PubMed: 17332749]
18. Kaden D, Voigt P, Munter LM, Bobowski KD, Schaefer M, Multhaup G. Subcellular localization and dimerization of APLP1 are strikingly different from APP and APLP2. J Cell Sci. 2009; 122:368–377. [PubMed: 19126676]
19. Wang Y, Ha Y. The X-ray structure of an antiparallel dimer of the human amyloid precursor protein E2 domain. Mol Cell. 2004; 15:343–353. [PubMed: 15304215]
20. Dahms SO, Hoefgen S, Roeser D, Schlott B, Guhrs KH, Than ME. Structure and biochemical analysis of the heparin-induced E1 dimer of the amyloid precursor protein. Proc Natl Acad Sci U S A. 2010; 107:5381–5386. [PubMed: 20212142]
21. Gralle M, Oliveira CL, Guerreiro LH, McKinstry WJ, Galatis D, Masters CL, Cappai R, Parker MW, Ramos CH, Torriani I, Ferreira ST. Solution conformation and heparin-induced dimerization of the full-length extracellular domain of the human amyloid precursor protein. J Mol Biol. 2006; 357:493–508. [PubMed: 16436282]

22. Rossjohn J, Cappai R, Feil SC, Henry A, McKinstry WJ, Galatis D, Hesse L, Multhaup G, Beyreuther K, Masters CL, Parker MW. Crystal structure of the N-terminal, growth factor-like domain of Alzheimer amyloid precursor protein. Nat Struct Biol. 1999; 6:327–331. [PubMed: 10201399]

23. Keil C, Huber R, Bode W, Than ME. Cloning, expression, crystallization and initial crystallographic analysis of the C-terminal domain of the amyloid precursor protein APP. Acta Crystallogr Sect D: Biol Crystallogr. 2004; 60:1614–1617. [PubMed: 15333934]

24. Dulubova I, Ho A, Huryeva I, Sudhof TC, Rizo J. Three-dimensional structure of an independently folded extracellular domain of human amyloid-beta precursor protein. Biochemistry. 2004; 43:9583–9588. [PubMed: 15274612]

25. Hoopes JT, Liu X, Xu X, Demeler B, Folta-Stogniew E, Li C, Ha Y. Structural characterization of the E2 domain of APL-1, a Caenorhabditis elegans homolog of human amyloid precursor protein, and its heparin binding site. J Biol Chem. 2010; 285:2165–2173. [PubMed: 19906646]

26. McCoy AJ, Grosse-Kunstleve RW, Adams PD, Winn MD, Storoni LC, Read RJ. Phaser crystallographic software. J Appl Crystallogr. 2007; 40:658–674. [PubMed: 19461840]

27. Pape T, Schneider TR. HKL2MAP: a graphical user interface for macromolecular phasing with SHELX programs. J Appl Crystallogr. 2004; 37:843–844.

28. Brunger AT, Adams PD, Clore GM, DeLano WL, Gros P, Grosse-Kunstleve RW, Jiang JS, Kuszewski J, Nilges M, Pannu NS, Read RJ, Rice LM, Simonson T, Warren GL. Crystallography & NMR system: A new software suite for macromolecular structure determination. Acta Crystallogr Sect D: Biol Crystallogr. 1998; 54:905–921. [PubMed: 9757107]

29. Winn MD, Murshudov GN, Papiz MZ. Macromolecular TLS refinement in REFMAC at moderate resolutions. Methods Enzymol. 2003; 374:300–321. [PubMed: 14696379]

30. Jones TA, Zou JY, Cowan SW, Kjeldgaard M. Improved methods for building protein models in electron density maps and the location of errors in these models. Acta Crystallogr, Sect A: Found Crystallogr. 1991; 47(Pt 2):110–119.

31. Otwinowski Z, Minor W. Processing of x-ray diffraction data collected in oscillation mode. Methods Enzymol. 1997; 276:307–326.

32. Emsley P, Lohkamp B, Scott WG, Cowtan K. Features and development of Coot. Acta Crystallogr Sect D: Biol Crystallogr. 2010; 66:486–501. [PubMed: 20383002]

33. Demeler, B. UltraScan: A Comprehensive Data Analysis Software Package for Analytical Ultracentrifugation Experiments. In: Scott, D.; Harding, S.; Rowe, A., editors. Modern Analytical Ultracentrifugation: Techniques and Methods. Royal Society of Chemistry; Cambridge, U.K: 2005. p. 210-229.

34. Demeler, B. UltraScan: A comprehensive data analysis software package for analytical ultracentrifugation experiments. 2010. http://www.utrascan.uthscsa.edu/

35. Brookes E, Demeler B. Parallel computational techniques for the analysis of sedimentation velocity experiments in UltraScan. Colloid Polym Sci. 2008; 286:138–148.

36. Brookes, EH.; Boppana, RV.; Demeler, B. Proceedings of the 2006 ACM/IEEE conference on Supercomputing. ACM; Tampa, Florida: 2006. Computing large sparse multivariate optimization problems with an application in biophysics; p. 81

37. Brookes E, Cao W, Demeler B. A two-dimensional spectrum analysis for sedimentation velocity experiments of mixtures with heterogeneity in molecular weight and shape. Eur Biophys J. 2010; 39:405–414. [PubMed: 19247646]

38. Demeler B, van Holde KE. Sedimentation velocity analysis of highly heterogeneous systems. Anal Biochem. 2004; 335:279–288. [PubMed: 15556567]

39. Brookes, E.; Demeler, B. Genetic Algorithm Optimization for Obtaining Accurate Molecular Weight Distributions from Sedimentation Velocity Experiments. In: Wandrey, C.; Cölfen, H., editors. Analytical Ultracentrifugation VIII. Springer; Berlin/Heidelberg: 2006. p. 33-40.

40. Brookes, EH.; Demeler, B. Proceedings of the 9th annual conference on Genetic and evolutionary computation. ACM; London, England: 2007. Parsimonious regularization using genetic algorithms applied to the analysis of analytical ultracentrifugation experiments; p. 361-368.

41. Demeler B, Brookes E. Monte Carlo analysis of sedimentation experiments. Colloid Polym Sci. 2008; 286:129–137.

42. Demeler B, Brookes E, Wang R, Schirf V, Kim CA. Characterization of reversible associations by sedimentation velocity with UltraScan. Macromol Biosci. 2010; 10:775–782. [PubMed: 20486142]

43. Cao W, Demeler B. Modeling analytical ultracentrifugation experiments with an adaptive space-time finite element solution for multicomponent reacting systems. Biophys J. 2008; 95:54–65. [PubMed: 18390609]

44. Jin LW, Ninomiya H, Roch JM, Schubert D, Masliah E, Otero DA, Saitoh T. Peptides containing the RERMS sequence of amyloid beta/A4 protein precursor bind cell surface and promote neurite extension. J Neurosci. 1994; 14:5461–5470. [PubMed: 8083748]

45. Popp GM, Graebert KS, Pietrzik CU, Rosentreter SM, Lemansky P, Herzog V. Growth regulation of rat thyrocytes (FRTL-5 cells) by the secreted ectodomain of beta-amyloid precursor-like proteins. Endocrinology. 1996; 137:1975–1983. [PubMed: 8612538]

46. Beher D, Hesse L, Masters CL, Multhaup G. Regulation of amyloid protein precursor (APP) binding to collagen and mapping of the binding sites on APP and collagen type I. J Biol Chem. 1996; 271:1613–1620. [PubMed: 8576160]

47. Mok SS, Sberna G, Heffernan D, Cappai R, Galatis D, Clarris HJ, Sawyer WH, Beyreuther K, Masters CL, Small DH. Expression and analysis of heparin-binding regions of the amyloid precursor protein of Alzheimer's disease. FEBS Lett. 1997; 415:303–307. [PubMed: 9357988]

48. Kraulis P. MOLSCRIPT: a program to produce both detailed and schematic plots of protein structures. J Appl Crystallogr. 1991; 24:946–950.

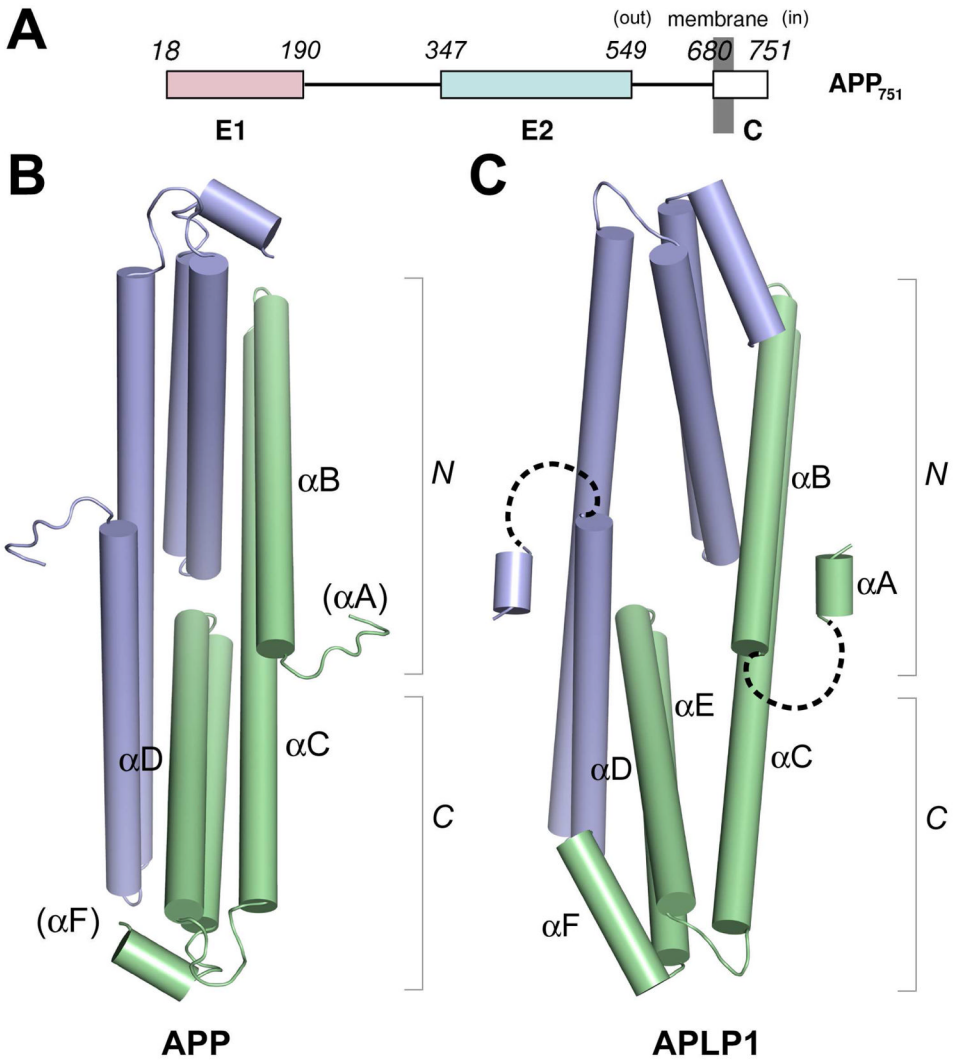

Figure 1.

The E2 domains of APP and APLP1 have similar dimeric structures. (**A**) The domain structure of APP. The residue numbers shown above the diagram are according to the common APP isoform-751. (**B**) The structure of the E2 domain of APP in crystal form “B”. Helix αA is disordered in the crystal lattice. The two protein protomers are shown in different colors. Helices are shown as cylinders. The two subdomains (N, C) are also labeled. (**C**) The structure of the E2 domain of APLP1. In the crystal, helix αA is domain swapped. Shown here are the corresponding helices from neighboring molecules (the loop connecting αA to αB is represented by the dashed line). These illustrations and those in Fig. 3C and Fig. 5 were generated by *PyMOL*.

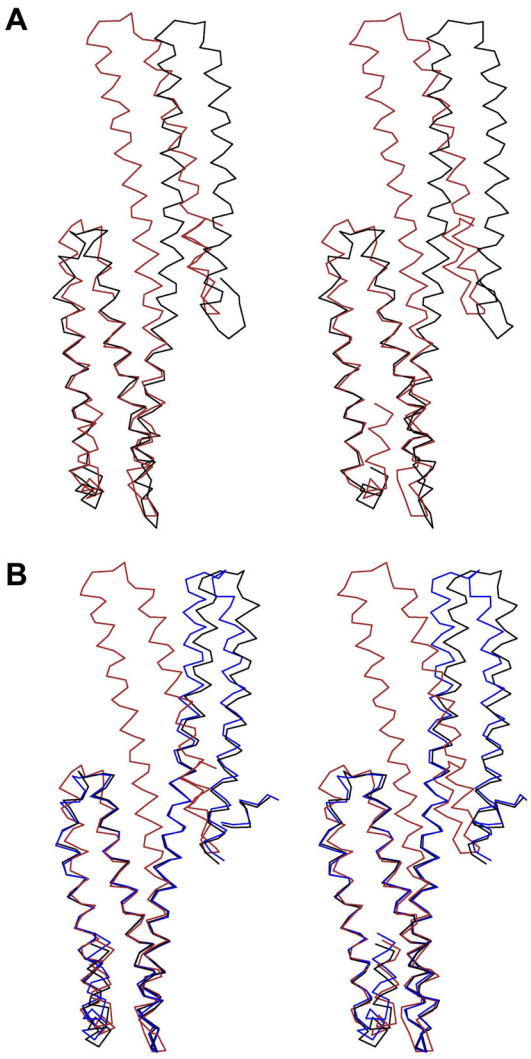

Figure 2.

Differences at the tertiary structural level. (**A**) Comparison between the two APP crystal forms. The new structure (black) is superimposed onto the C-terminal subdomain of the original APP structure (red; PDB entry 1rw6). The Cα-traces are shown in stereo pairs. (**B**) Comparison between APP (red; the original structure 1rw6) and APLP1 (blue and black). The two copies of APLP1 in the asymmetric unit are slightly different in their inter-subdomain angles. These images and those in Fig. 3A-B were generated by *Molscript* (48).

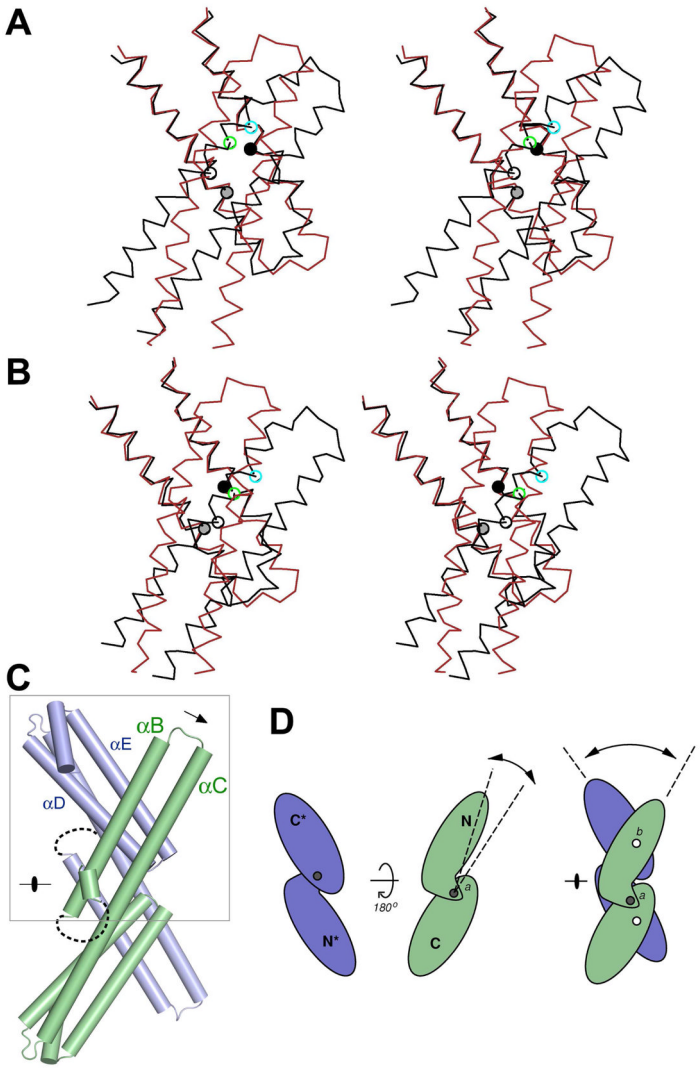

Figure 3.

Differences at the dimeric interface. (**A**) Comparison between the two APP crystal forms. The new structure (black) is superimposed onto αD and αE of the original structure (red; PDB entry 1rw6). The helices that "moved" correspond to αB and αC of the second protomer across the dimeric interface. The Cα-traces are shown in stereo pairs. Grey circle, Leu-490*; black circle, Leu-515*; white circle, Met-387; green circle, Met-391; blue circle, Trp-394. αB and αC appear to pivot around Met-387. (**B**) Comparison between APP (red; the original structure 1rw6) and APLP1 (black). Grey circle, Leu-428*; black circle, Leu-453*; white circle, Ile-325; green circle, Met-329; blue circle, Trp-332. (**C**) A side view of the APLP1 dimer. The arrow indicates the "rotation" of αB/αC relative to αD/αE across the dimeric interface in APLP1 when compared to APP. The grey box indicates the region shown in **A** and **B**. (**D**) In this model, each subdomain is represented by a single oval-shaped object. Within each protomer, the two subdomains are connected at point "a" (grey circle), and can rotate about it (dashed lines). The dimer is held together by two joints (white circles; "b"). The two subdomains across the dimeric interface can only rotate about "b" (dashed lines).

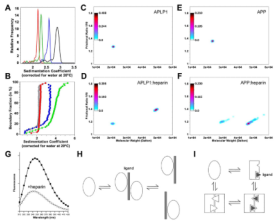

Figure 4.

Heparin binding enhances E2 dimerization. (**A**) van Holde-Weischet g(s) graphs for the E2 domain of APLP1 for a range of protein concentrations (red, 3.2μM; green, 6.6μM; blue, 32μM; black, 66μM). When the protein concentration was raised from 3.2μM (0.31 OD at 230nm) to 66μM (0.76 OD at 280nm), the major peak gradually shifted from 2.2 S to 2.9 S. This result is due to the rapid exchange between monomers (24.9 kDa) and dimers (49.8 kDa), and was confirmed by fitting the data to a reversible monomer-dimer model (42, 43). This observation suggests that reversible dimerization is driven by mass action even in the absence of ligand. (**B**)-(**F**), Sedimentation velocity experiments of the E2 domains of APLP1 and APP in the presence and absence of heparin. Integral van Holde-Weischet s-value distributions (**B**: grey, APLP1; blue, APLP1+100μM heparin; red, APP; green, APP+100μM heparin) and genetic algorithm-Monte Carlo results (**C:** APLP1, **D:** APLP1+100μM heparin, **E:** APP, **F:** APP+100μM heparin) reveal enhanced dimerization when heparin is present. **C-F:** The y-axis shows the frictional ratio (f/f_0), which measures the globularity of the solute. An f/f_0 value of unity corresponds to a spherical molecule. The color gradients indicate optical density at 230nm. For clarity, only the monomer-dimer molecular weight range is shown in **C-F**. The full sedimentation range is shown in B. The protein loading concentration is approximately 3μM in all experiments shown in panels **B-F**. (**G**) Heparin binding causes a decrease of APLP1 E2 fluorescence intensity. Filled circles, protein alone (3μM); open circles, protein plus heparin (6μM). (**H**) A model where the heparin-induced dimer does not have a protein:protein interface. Additional ligand may dissociate the dimer by competing for the ligand binding site. Oval, protein; grey bar, ligand. (I) In this model the dimer is strengthened by protein:protein contact and by additional interactions between heparin (represented by the grey triangles) and the protein protomer across the dimeric interface (small indentation). Ligand may also change the conformation of the protein (oval to rectangle) to facilitate the formation of a protein:protein interface.

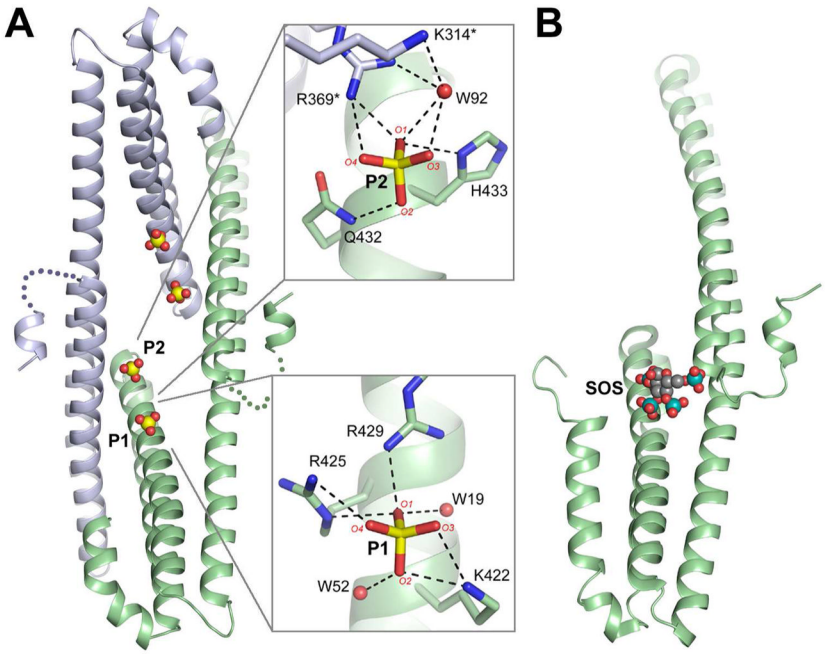

Figure 5.

The phosphate binding sites. (**A**) The P1 and P2 binding sites. The dashed lines represent hydrogen bonds. Red spheres represent water molecules. The two protein protomers are shown in different colors. (**B**) A similar view of the monomeric structure of *C. elegans* APL-1 in complex with sucrose octasulfate (25).

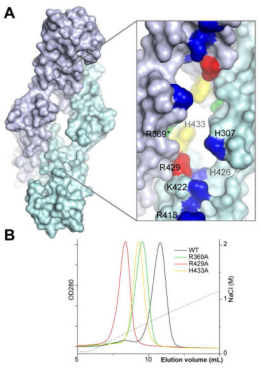

Figure 6.

Mutational mapping of the heparin binding site. (**A**) A surface representation of the heparin binding site mapped by mutagenesis. The two protein protomers are shown in different colors. (**B**) The elution profiles of wild-type and mutant proteins from a heparin column. The dashed line represents salt gradient.

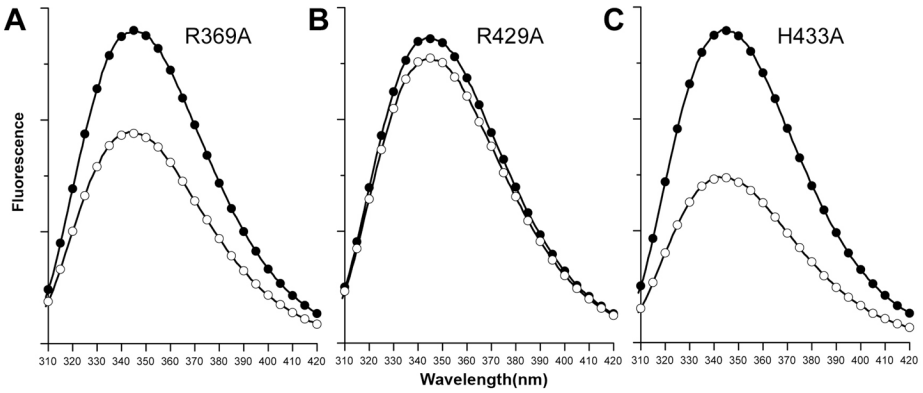

Figure 7.

The heparin-binding mutants show decreased dimerization. (**A**) R369A. (**B**) R429A. (**C**) H433A. These experiments were conducted under exactly the same conditions as that for the wildtype protein (Fig. 4G). Filled circles, mutant protein alone; open circles, protein plus heparin.

Table 1

Crystallographic statistics.

Data collection	**APP (crystal form "B")**	**APLP1**
Space group	$P2_12_12$	$P2_12_12_1$
Cell dimensions (Å)	a=115.0, b=40.1, c=58.4	a=74.9, b=81.3, c=89.7
Wavelength (Å)	1.1400	1.075
[a] Resolution (Å)	40.0–3.2 (3.31–3.20)	40.0–2.1 (2.18–2.10)
Observed reflections	65,248	303,135
Unique reflections	4,888	32,194
Redundancy	13.3	9.4
[a] Completeness (%)	99.6 (100.0)	100.0 (100.0)
$[a]_{<I/\sigma>}$	14.0	16.5
[a,b] R_{merge}	0.081 (0.368)	0.070 (0.402)
Refinement		
Resolution (Å)	40.0–3.2	40.0–2.1
[c] R_{work}/R_{free}	0.297/0.380	0.208/0.244
Number of atoms		
Protein	1,226	3,170
Metal ion	1	0
Phosphate ion	0	20
Water	36	277
B-factors		
Protein	110	46
Metal ion	92	-
Phosphate ion	-	56
Water	101	55
R.m.s. deviations		
Bond lengths (Å)	0.009	0.007
Bond angle (°)	1.57	1.06

[a] Highest resolution shell is shown in parentheses.

[b] $R_{merge} = \Sigma \mid I_i - \langle I \rangle \mid / \Sigma I_i$

[c] $R_{work} = \Sigma \mid F_o - F_c \mid / \Sigma F_o$. R_{free} is the cross-validation R factor for the test set of reflections (10% of the total) omitted in model refinement.